


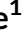




## ORIGINAL ARTICLE

# A role for Mitochondrial Rho GTPase 1 (MIRO1) in motility and membrane dynamics of peroxisomes

Inês G. Castro<sup>1</sup>  | David M. Richards<sup>2</sup> | Jeremy Metz<sup>1</sup>  | Joseph L. Costello<sup>1</sup>  |  
Josiah B. Passmore<sup>1</sup>  | Tina A. Schrader<sup>1</sup> | Ana Gouveia<sup>3</sup> | Daniela Ribeiro<sup>3</sup>  |  
Michael Schrader<sup>1</sup> 

<sup>1</sup>Biosciences, University of Exeter, Exeter, UK

<sup>2</sup>LSI, University of Exeter, Exeter, UK

<sup>3</sup>Institute of Biomedicine, University of Aveiro, Aveiro, Portugal

## Correspondence

Michael Schrader, Biosciences, University of Exeter, Exeter EX4 4QD, UK.  
Email: m.schrader@exeter.ac.uk

## Present address

Inês G. Castro, Department of Molecular Genetics, Weizmann Institute of Science, Rehovot 7610001, Israel.

## Funding information

Fundação para a Ciência e a Tecnologia, Grant/Award numbers: PTDC/BIABCM/118605/2010; SFRH/BD/81223/2011, SFRH/BPD/77619/2011; Wellcome Trust, Grant/Award numbers: WT097835MF; WT105618MA; Biotechnology and Biological Sciences Research Council, Grant/Award numbers: BB/K006231/1, BB/N01541X/1; Medical Research Council, Grant/Award number: MR/P022405/1

Peroxisomes are dynamic organelles which fulfil essential roles in lipid and ROS metabolism. Peroxisome movement and positioning allows interaction with other organelles and is crucial for their cellular function. In mammalian cells, such movement is microtubule-dependent and mediated by kinesin and dynein motors. The mechanisms of motor recruitment to peroxisomes are largely unknown, as well as the role this plays in peroxisome membrane dynamics and proliferation. Here, using a combination of microscopy, live-cell imaging analysis and mathematical modelling, we identify a role for Mitochondrial Rho GTPase 1 (MIRO1) as an adaptor for microtubule-dependent peroxisome motility in mammalian cells. We show that MIRO1 is targeted to peroxisomes and alters their distribution and motility. Using a peroxisome-targeted MIRO1 fusion protein, we demonstrate that MIRO1-mediated pulling forces contribute to peroxisome membrane elongation and proliferation in cellular models of peroxisome disease. Our findings reveal a molecular mechanism for establishing peroxisome-motor protein associations in mammalian cells and provide new insights into peroxisome membrane dynamics in health and disease.

## KEYWORDS

mathematical modelling, membrane protrusion, microtubule, MIRO1, organelle motility, peroxisome, proliferation

## 1 | INTRODUCTION

Peroxisomes are dynamic, multifunctional organelles that vary in size, number and shape depending on cell type, environmental stimuli and metabolic demand,<sup>1</sup> but the underlying molecular mechanisms which govern this versatility are not fully understood. Similar to mitochondria, peroxisomes are oxidative organelles that fulfil important functions in lipid metabolism and ROS homeostasis rendering them essential for human health and development.<sup>2,3</sup> Peroxisomes metabolically cooperate and physically interact with a variety of subcellular organelles including the ER, mitochondria, lipid droplets and other

peroxisomes.<sup>4–6</sup> These functions require peroxisome positioning and movement within eukaryotic cells.

Whereas in yeast and plant cells peroxisome motility depends on actin filaments and myosin motors,<sup>7,8</sup> in mammalian cells peroxisomes move bidirectionally via microtubules, using both kinesin and dynein motors.<sup>9–12</sup> The shape and number of peroxisomes is controlled by PEX11 $\beta$ , a peroxisomal membrane protein, which induces elongation and remodelling of the peroxisomal membrane and acts as a GTPase activating protein on the large fission GTPase DNM1L.<sup>13–15</sup> Loss of PEX11 $\beta$  was recently linked to spindle misorientation and peroxisome mislocalisation in mitosis causing imbalances in epidermal differentiation.<sup>16</sup> These findings underline the importance of peroxisome multiplication, distribution and inheritance for cell fate decisions.

**Abbreviations:** TA, tail-anchored; TMD, transmembrane domain; WT, wild type; ROS, reactive oxygen species; ER, endoplasmic reticulum

This is an open access article under the terms of the Creative Commons Attribution License, which permits use, distribution and reproduction in any medium, provided the original work is properly cited.

© 2018 The Authors. Traffic published by John Wiley & Sons Ltd.

Although key factors required for peroxisome dynamics and multiplication have been identified, it is currently unclear to what extent cytoskeletal tracks, docking factors and pulling forces mediated by associated motor proteins contribute to these processes, in particular in mammals.<sup>17</sup> In baker's yeast, peroxisome distribution and inheritance depends on actin, the myosin motor Myo2 and specific adaptor proteins, Inp1 and Inp2, at the peroxisomal membrane.<sup>7</sup> Furthermore, the peroxins Pex3 and Pex19 have been found to interact with myosin motors.<sup>18,19</sup> In contrast, little is known about the recruitment of microtubule motors to peroxisomes in mammalian cells.<sup>20</sup>

Here, we identify the Ras GTPase MIRO1 as a potential adaptor for microtubule-based peroxisome motility in mammalian cells. MIRO proteins were initially identified on the outer mitochondrial membrane<sup>21</sup> where they, together with TRAK1/2, link the microtubule motors kinesin and dynein to mitochondria,<sup>22–25</sup> and play key roles in mitochondrial motility, homeostasis and inheritance.<sup>26,27</sup> Mammalian MIRO1 and MIRO2 share 60% similarity and an analogous structure containing 2 GTPase and 2 EF-hand calcium binding domains.<sup>21,28</sup> Studies on mammalian MIRO proteins have focused mainly on MIRO1 due to its clear role in mitochondrial motility, particularly in neurons.<sup>22,25</sup> Loss of MIRO1-directed mitochondrial movement and distribution result in neurological defects.<sup>26</sup> MIRO1-mediated mitochondrial positioning is also suggested to shape intracellular energy gradients required for cell migration.<sup>29</sup> We show that MIRO1 localises to peroxisomes and mitochondria, and alters peroxisome distribution and motility. Furthermore, we demonstrate that an exclusively peroxisome-targeted MIRO1 can mediate pulling forces which contribute to peroxisome membrane elongation and proliferation in a cell type-dependent manner. To better understand the versatility of peroxisomes in mammalian cells, we build a first mathematical model of peroxisome dynamics. This model helps to explain the underlying principles of peroxisome morphologies induced by MIRO1-mediated pulling forces and other factors which influence peroxisomal membrane dynamics.

## 2 | RESULTS

### 2.1 | MIRO1 is dually targeted to peroxisomes and mitochondria

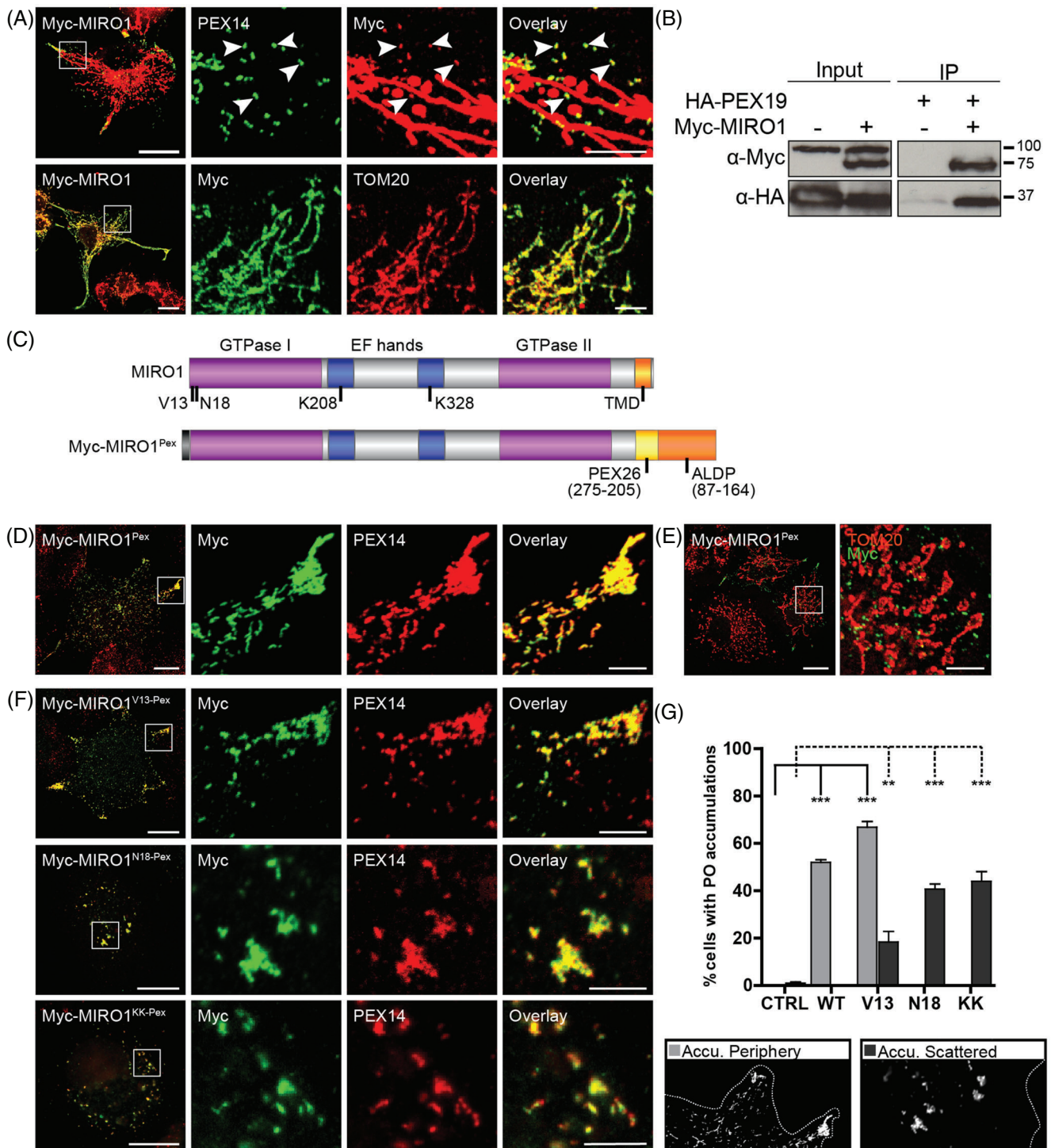
Previous studies revealed a dual mitochondrial and peroxisomal localisation of several C-tail-anchored (TA) membrane proteins including FIS1, MFF and GDAP1, which function in peroxisomal and mitochondrial division.<sup>30–33</sup> In a recent study on the targeting of TA proteins to different organelles, we provided preliminary evidence for a dual peroxisomal and mitochondrial localisation of the Ras GTPases MIRO1 and MIRO2.<sup>34</sup> MIRO1 was initially identified on the outer mitochondrial membrane,<sup>21</sup> and forms a protein complex with TRAK1/2 that includes both kinesin and dynein motors, promoting mitochondrial movement through the microtubule cytoskeleton.<sup>22–25</sup> A dual mitochondrial and peroxisomal localisation of MIRO1 was confirmed by immunofluorescence after expression of Myc-MIRO1 in COS-7 cells (Figure 1A). Furthermore, we previously reported

endogenous MIRO1 in highly purified peroxisomal and mitochondrial fractions,<sup>34</sup> in agreement with proteomics data.<sup>35,36</sup>

The targeting of all known TA proteins to peroxisomes requires the peroxisomal import receptor/chaperone PEX19.<sup>34</sup> For MIRO1, PEX19 binding was shown by immunoprecipitation after co-expression of Myc-MIRO1 and HA-PEX19 in COS-7 cells (Figure 1B) suggesting a role for PEX19 in the targeting of MIRO1 to peroxisomes. Additionally, in a high-throughput interaction study, MIRO1 was identified as a PEX19 interaction partner.<sup>37</sup> These findings are also consistent with the known organelle targeting signals: MIRO1 possesses a transmembrane domain (TMD) with relatively low hydrophobicity (GRAVY, 1.3) and a moderate net charge in the tail region (1.9), which based on our previous work would be indicative of a TA protein that localises predominantly to mitochondria but has a potential for peroxisomal targeting.<sup>34</sup> Overall, our findings support a dual localisation of MIRO1 at mitochondria and peroxisomes.

### 2.2 | MIRO1 alters peroxisome distribution in COS-7 cells

MIRO1 has been shown to play a key role in mitochondrial motility and distribution in mammalian cells.<sup>26</sup> To determine if MIRO1 also plays a role in peroxisome positioning we expressed Myc-tagged wild type (WT) and mutated versions in COS-7 cells, and analysed their effect on peroxisome distribution (Figures 1A,C and S1). As previously described,<sup>21,38</sup> the expression of Myc-MIRO1 resulted in abnormal mitochondrial morphologies (Figures 1A and S1). To avoid potential secondary effects due to dysfunctional mitochondria, we generated an exclusively peroxisomal set of MIRO1 proteins by altering the C-terminal TMD using a previously described PEX26/ALDP construct (Figure 1C).<sup>39</sup> Expression of the resulting Myc-MIRO1<sup>Pex</sup> fusion protein in COS-7 cells revealed an exclusively peroxisomal localisation, with no effects on mitochondrial morphology and distribution (Figure 1D,E). Peroxisomes in COS-7 cells usually distribute uniformly throughout the cytoplasm.<sup>30,40</sup> Interestingly, expression of Myc-MIRO1<sup>Pex</sup> or Myc-MIRO1<sup>V13-Pex</sup>, a constitutively active GTPase mutant, induced peroxisome redistribution and accumulation at the cell periphery (Figure 1D,F,G). On the other hand, expression of dominant negative Myc-MIRO1<sup>N18-Pex</sup> and EF-hand mutant Myc-MIRO1<sup>KK-Pex</sup> resulted in peroxisome accumulations which were scattered throughout the cytoplasm (Figure 1F,G). Comparable results were obtained with the dually targeted MIRO1 versions (Figure S1B). Myc-MIRO1<sup>ΔTM</sup>, a version lacking the TMD/tail sequence, localised to the cytoplasm and had no effect on peroxisome distribution, indicating that membrane anchorage is required for MIRO1 function (Figure S1). Furthermore, depolymerisation of microtubules with nocodazole in Myc-MIRO1<sup>Pex</sup> expressing cells abolished accumulation of peroxisomes in the cell periphery, suggesting that an intact microtubule cytoskeleton is required for peroxisome distribution via MIRO1 (Figure S2A). Our findings indicate that, similar to its role on mitochondria, MIRO1 can alter peroxisome distribution and positioning by affecting microtubule-dependent peroxisome motility.



**FIGURE 1** MIRO1 is targeted to peroxisomes and alters their distribution in COS-7 cells. A, COS-7 cells were transfected with Myc-MIRO1, fixed and stained against Myc, and PEX14 or TOM20. B, Co-immunoprecipitation from COS-7 cells expressing HA-PEX19 and Myc-MIRO1, using  $\alpha$ -Myc-conjugated agarose beads. HA-PEX19 only co-immunoprecipitated in the presence of Myc-MIRO1. Higher band in  $\alpha$ -Myc Input is unspecific. Input—10% of total cell lysates, IP—immunoprecipitation. C, Schematic view of MIRO1 domains and mutation sites and the Myc-MIRO1<sup>PEX</sup> construct. D-F, COS-7 cells were transfected with Myc-MIRO1<sup>PEX</sup> constructs and stained against Myc and PEX14 or TOM20; D, Myc-MIRO1<sup>PEX</sup> was exclusively targeted to peroxisomes and induced redistribution to the cell periphery (E) without affecting mitochondrial morphology and distribution; F, mutated Myc-MIRO1<sup>PEX</sup> proteins were exclusively targeted to peroxisomes and induced the formation of peroxisomal accumulations in the cell periphery (V13) or scattered (V13, N18 and KK). G, Quantitative analysis of peroxisome distribution as shown in D-F. Cells with peroxisomal accumulations in the periphery or scattered were counted. Values represent mean  $\pm$  SEM of 3 independent experiments (100 replicates per experiment per condition; \*\*  $P < .01$ ; \*\*\*  $P < .001$ ; one-way ANOVA with post hoc Tukey test vs control). Bars, 20  $\mu$ m (overview), 5  $\mu$ m (magnification)

### 2.3 | Peroxisomal MIRO1 increases movement of peroxisomes

To quantify the effect of MIRO1 expression on peroxisome motility, live-cell imaging experiments were performed with COS-7 cells expressing Myc-MIRO1<sup>V13-Pex</sup> and the peroxisome marker EGFP-SKL (Figure 2A-C; Videos S1 and S2). To measure movement, peroxisomes were automatically detected and tracked using a customised in-house algorithm.<sup>41</sup> To visualise displacement, 100 trajectories were randomly sampled and plotted from a central point (Figure 2A). Expression of Myc-MIRO1<sup>V13-Pex</sup> significantly increased peroxisome displacement. Figure 2B displays the empirical cumulative distribution function (ECDF) of the instantaneous peroxisome speeds for all peroxisomes analysed with each point of the curve corresponding to a single movement. For this analysis, all speed values above 0.24  $\mu\text{m/s}$  were considered microtubule-dependent movements as previously described.<sup>42</sup> A significant increase in the number of fast moving peroxisomes can be observed in cells expressing Myc-MIRO1<sup>V13-Pex</sup> (Figure 2B,C; Videos S1 and S2). Whereas in control cells 5.2%  $\pm$  0.7% of peroxisomes moved in a microtubule-dependent manner, in cells expressing Myc-MIRO1<sup>V13-Pex</sup> this number increased to 14.0%  $\pm$  2.0% (Figure 2C). Imaging of peroxisome accumulations at the cell periphery revealed that while the organelles appear to be confined to a relatively restricted area of the cell, peroxisomes regularly move within these accumulations, revealing dynamic interactions (Video S2). To examine the effect of a loss of MIRO1 function on peroxisome distribution and motility, we analysed MIRO1 KO MEFs (Figure S2B-E). These cells have an altered mitochondrial distribution but peroxisome morphology and distribution appeared to be unaffected.<sup>43</sup> In agreement with those findings, we did not detect any alterations in peroxisome distribution (Figure S2C) or motility (Figure S2D,E). These findings indicate that when targeted to peroxisomes in COS-7 cells, active MIRO1, a known adaptor for the microtubule plus-end motor kinesin, can redistribute peroxisomes to the cell periphery (where microtubule plus ends are located) in a microtubule-dependent manner. However, MIRO1 may not be the only adaptor for microtubule-dependent motor proteins at peroxisomes, as its loss is apparently not essential to maintain peroxisome distribution and motility. It is possible that MIRO2, which also localises to peroxisomes,<sup>34</sup> can complement loss of MIRO1. Furthermore, peroxisomes may tether to or “hitch-hike” other moving organelles to maintain their distribution. The latter process has been observed in filamentous fungi.<sup>44</sup>

### 2.4 | MIRO1 induces peroxisome proliferation in human skin fibroblasts

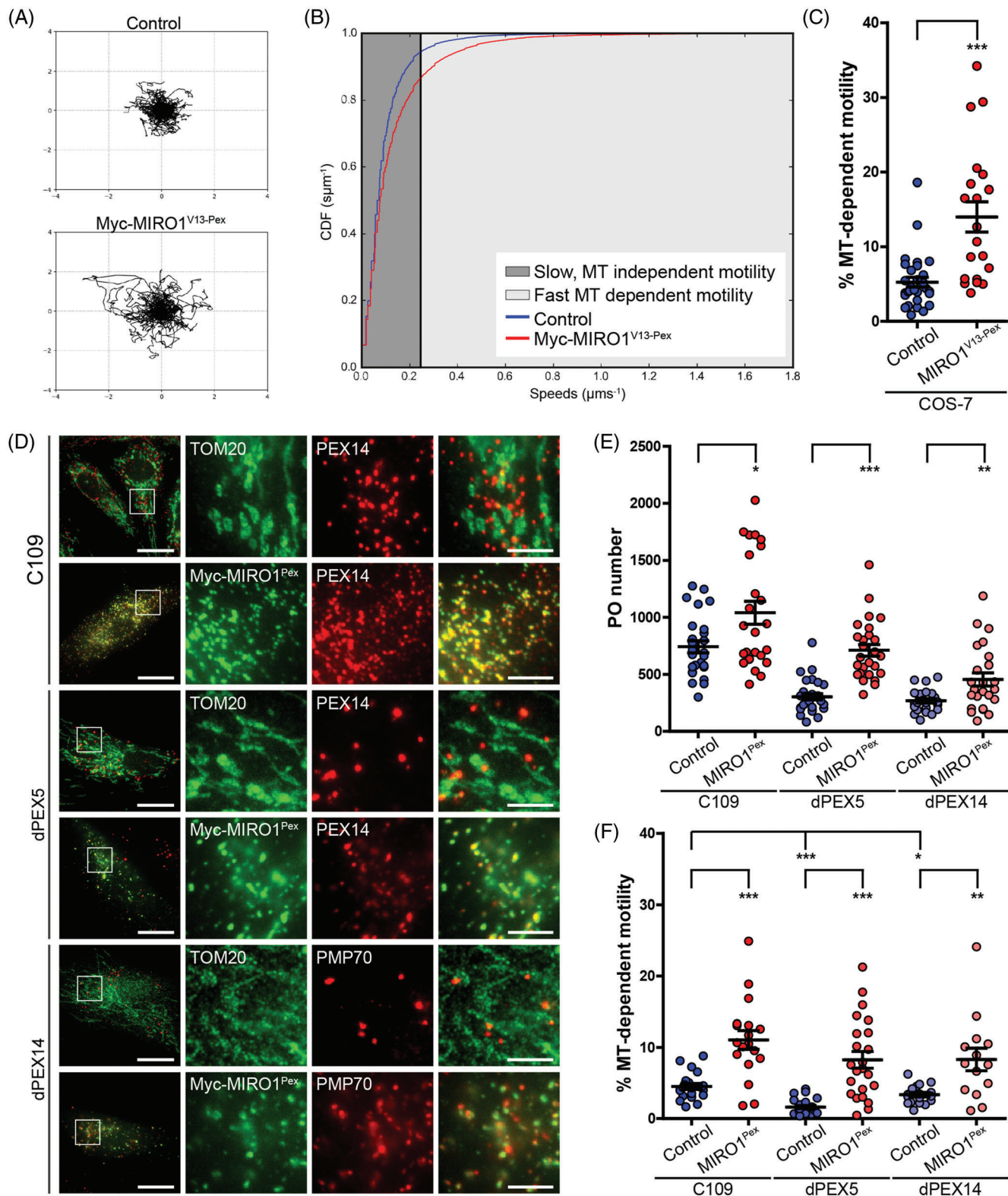
The peroxisome-targeted MIRO1 represents a new tool to manipulate peroxisome motility and to exert motor-driven pulling forces at peroxisomes under control and disease conditions. Peroxisomes in fibroblasts from patients with peroxisomal disorders are often enlarged and reduced in number, and tend to cluster and detach from microtubules.<sup>45</sup> We first expressed Myc-MIRO1<sup>Pex</sup> in human

skin fibroblasts from a healthy control and examined its effect on the peroxisomal compartment (Figure 2D). Surprisingly, in these cells peroxisomes did not accumulate at the cell periphery but instead proliferated, presenting a significant increase in number (mean peroxisome number/cell: control 740  $\pm$  50; Myc-MIRO1<sup>Pex</sup> 1040  $\pm$  100,  $n = 24$ ; Figure 2E). In addition, the percentage of motile peroxisomes that moved in a microtubule-dependent manner was significantly increased (Figure 2F; Figure S2F; Videos S3 and S4). These findings indicate that MIRO1-bound motor proteins can exert forces at peroxisomes, which result in peroxisome division, thus increasing peroxisome number. Separation by pulling forces is only possible when the peroxisome is tethered to another structure, as it would otherwise simply move in the direction of the pulling force (Figure 4B). This untethered motion is observed in COS-7 cells, where MIRO1 expression accumulates peroxisomes in the cell periphery where microtubule-plus ends are located (Figures 1 and 4B). We recently revealed that peroxisome-ER membrane contacts are mediated by peroxisomal ACBD5 that interacts with ER-resident VAPB to form a peroxisome-ER tether.<sup>46</sup> Loss of ACBD5 increased the movement of peroxisomes in human skin fibroblasts, indicating that peroxisome-ER membrane contacts restrict peroxisome motility. In line with this, our analyses reveal that the percentage of fast moving peroxisomes in control fibroblasts is lower than that in control COS-7 cells (4.5%  $\pm$  0.4% vs 5.2%  $\pm$  0.7%). We suggest that peroxisome-ER tethering is cell-type specific and that MIRO1/motor-mediated pulling forces can induce peroxisome proliferation in fibroblasts, whereas in COS-7 cells peroxisomes are dragged towards the cell periphery (Figure 4B). These findings indicate that a close interplay between tethering and motile forces modulates not only peroxisome distribution but also proliferation.

To analyse the impact of MIRO1 expression on peroxisomes in patient fibroblasts, we expressed Myc-MIRO1<sup>Pex</sup> in PEX5 and PEX14 deficient cells. PEX5 and PEX14 are proteins of the peroxisomal matrix protein import machinery, and loss of function leads to “empty” membrane structures (so called “ghosts”) that lack peroxisomal enzymes and are metabolically inactive. Peroxisomes in those cells are often enlarged and reduced in number (Figure 2D). Expression of Myc-MIRO1<sup>Pex</sup> in both PEX5 and PEX14 deficient cells induced peroxisome proliferation, but many peroxisomes remained enlarged (Figure 2D,E). MIRO1 expression also significantly increased peroxisome motility in patient cells (Figure 2F; Figure S2G-H), most prominently for the smaller peroxisomes (Videos S5-S8). In contrast to a recent report, we observed that peroxisomes in PEX14 deficient cells are motile.<sup>47</sup> These findings show that MIRO1-mediated pulling forces can at least partially induce the proliferation of metabolically inactive peroxisomes, indicating that membrane components are the most relevant factors for this process.

### 2.5 | Peroxisome-targeted MIRO1 promotes the formation of extended membrane protrusions in PEX5 deficient fibroblasts

Peroxisomes are highly dynamic organelles that can be found as spherical or elongated structures and also form membrane



**FIGURE 2** MIRO1 expression increases microtubule-dependent peroxisome motility in mammalian cells and induces peroxisome proliferation in human skin fibroblasts. A-C, Myc-MIRO1<sup>V13-Pex</sup> expression increases peroxisome movement. COS-7 cells were transfected with Myc-MIRO1<sup>V13-Pex</sup> and EGFP-SKL. For each cell, 500 stacks of 5 planes were obtained over time, and peroxisomes detected and tracked using an automated algorithm. A, Trajectory plots. Hundred peroxisome trajectories were retrieved for each condition and the first 20 time-frames plotted starting at a centre. B, CDF plot. Instantaneous trajectory speed profiles were estimated by calculating distance moved between each time point in the trajectory. These speeds were pooled and converted to an ECDF. By pooling speeds for all data sets for a given condition, a single ECDF was generated for each. A threshold of 0.24  $\mu\text{m/s}$  was defined for microtubule-dependent motility. C, Percentage of fast moving peroxisomes per cell in control and Myc-MIRO1<sup>V13-Pex</sup> expressing cells. Values represent mean  $\pm$  SEM of 20 to 30 cells from 3 independent experiments (\*\*\*  $P < .001$ ; two-tailed unpaired  $t$  test vs control cells). D, C109, dPEX5 and dPEX14 cells were transfected with Myc-MIRO1<sup>Pex</sup>, fixed and stained against PEX14, TOM20, PMP70 and Myc. Expression of Myc-MIRO1<sup>Pex</sup> induces peroxisome proliferation. E-F, C109, dPEX5 and dPEX14 cells

protrusions. These membrane alterations are suggested to contribute to peroxisome formation via division of elongated organelles, and to enable organelle crosstalk.<sup>1,48</sup> To what extent microtubule motors and pulling forces contribute to peroxisome membrane dynamics is unclear, as peroxisome elongation is unexpectedly promoted by microtubule-depolymerising drugs, and peroxisome division can occur in the absence of microtubules.<sup>9,49</sup> In PEX5 deficient fibroblasts expressing Myc-MIRO1<sup>Pex</sup>, we observed long membrane protrusions emanating from large, spherical peroxisomes and following linear tracks with sporadic bends (Figure 3A). These membrane protrusions co-localised with microtubules, indicating their formation is promoted by MIRO1/motor generated pulling forces along microtubules (Figure 3B). Our observations also suggest the existence of as yet unidentified docking proteins which link peroxisomes to microtubules, and would facilitate the bending and directional changes we observe in the membrane protrusions. To analyse the dynamics of peroxisomal membrane protrusions, we performed time-lapse analyses of PEX5 deficient cells expressing Myc-MIRO1<sup>Pex</sup> (Figure 3C). We revealed that protrusions originating from large peroxisomes grow at varying speeds, generally form straight lines in a single direction (Figure 3C-E; Video S9) and occasionally appear to interact with other peroxisomes (Figure 3C). Transient peroxisome interactions, which may contribute to organelle crosstalk, have been previously reported.<sup>42</sup> Interestingly, these protrusions can sometimes quickly retract, suggesting that the peroxisomal membrane has elastic properties that are largely unexplored (Figure 3C,D). A comparison of the surface area of a globular peroxisome from Zellweger fibroblasts (approximately 1  $\mu\text{m}$  in diameter)<sup>50</sup> with an elongated membrane protrusion (approximately 20  $\mu\text{m}$  in length, 80 nm in diameter)<sup>14,46</sup> indicates a 16-fold increase in the surface area of the protrusion. As it is unlikely that the globular peroxisome on its own can provide sufficient membrane lipids to generate such a protrusion, additional membrane lipids are likely provided by the ER. In support of this, we have recently revealed that peroxisome-ER membrane contacts have an impact on peroxisomal membrane expansion.<sup>46</sup> Whereas protrusions were not observed in control fibroblasts, they were formed in PEX5 and PEX14 deficient cells under control conditions, albeit more frequently in PEX5 deficient cells (Figure 3E). As peroxisomes are reduced in number in PEX5 and PEX14 deficient cells and are less motile than in controls, peroxisome protrusions may form to overcome those restrictions and to maintain organelle crosstalk. However, peroxisome metabolism is required to generate cellular lipids which are also necessary for peroxisome division and proliferation.<sup>51</sup> As PEX5 and PEX14 deficient cells lack peroxisomal metabolic functions, their ability to divide and proliferate peroxisomes is compromised,

which may explain the formation and frequency of membrane elongations (Figure 4B). Expression of Myc-MIRO1<sup>Pex</sup>, however, significantly increased the frequency and length of protrusions in PEX5 deficient but not in PEX14 deficient cells (Figure 3E), suggesting that loss of PEX14 could interfere with the stability of membrane protrusions.

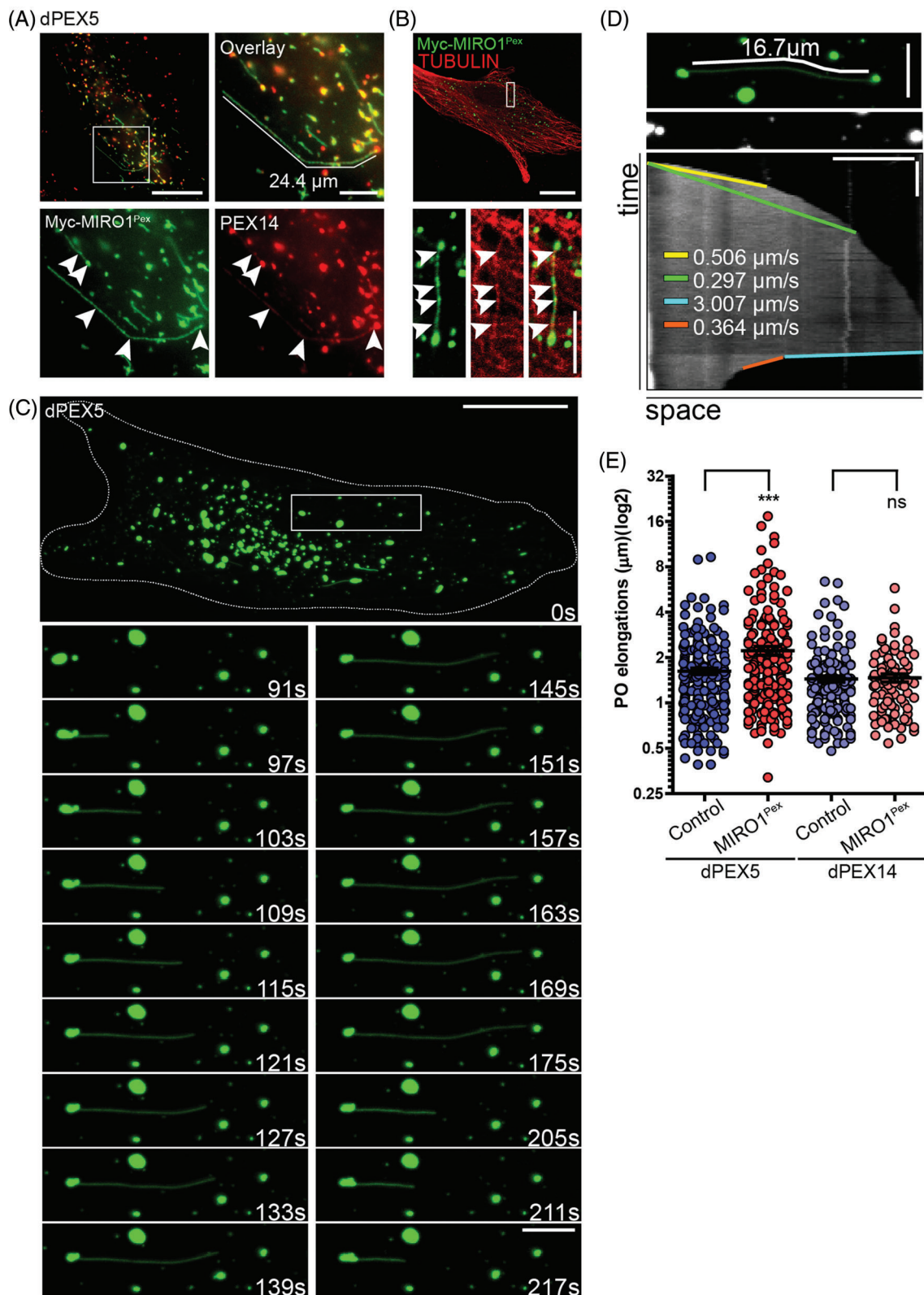
## 2.6 | A mathematical model of peroxisome dynamics

To further understand the mechanisms involved in peroxisome dynamics, we developed a simple mathematical model that describes their growth and division. We used a stochastic, population-based modelling approach that describes the morphology of a group of individual peroxisomes. Each peroxisome consists of a body of radius  $r$  with an optional elongation of length  $L$  and diameter  $w$  (Figure 4A(a)). The size of the body and elongation are controlled by 3 basic processes (Figure 4A(b)): (1) a membrane lipid flow rate to the body (eg, from the ER) (governed by rate  $\alpha$  and lipid flow constant  $\gamma$ ), (2) an elongation growth rate (governed by speed  $v$  and minimum radius  $r_{\text{min}}$ ) and (3) a division rate proportional to the elongation length (governed by rate  $\beta$  and minimum length  $L_{\text{min}}$ ). In addition, peroxisome turnover is controlled by the peroxisome mean lifetime  $\tau$ . This leads to a model that is applicable to a range of experimental conditions (see Supporting information for full model details). Using WT parameters, we obtained a phenotype that reflects the heterogeneous peroxisome population observed in mammalian cells in terms of number, average body size and average elongation length (Figure 4A(c)). The WT division rate  $\beta$  is sufficiently high, resulting in division of peroxisome elongations shortly after formation. When considering a block in peroxisome division by setting the division rate  $\beta$  to almost zero, the model exhibits reduced numbers of peroxisomes all of which contain long elongations (Figure 4A(d)). Such a scenario is observed in patient fibroblasts lacking MFF, the membrane adaptor for the fission GTPase Drp1, where we would expect division rates to be significantly reduced.<sup>52,53</sup> The fact that changing only one parameter can capture this dramatic change in phenotype gives confidence that the model is able to correctly describe the basic processes involved in peroxisomal growth and division.

Next, we examined overexpression of MIRO1 in WT cells. For fibroblasts, we modelled this as a large increase (by a factor of 10) in the elongation growth rate  $v$  accompanied by an increase in lipid flow (modelled by halving the lipid flow constant  $\gamma$ ). This leads to an increase in peroxisome number without a noticeable change in morphology, which is again explained by the fact that the WT division

---

were transfected with EGFP-ACBD5<sup>TMD-T</sup> (peroxisomal membrane marker) alone, or co-transfected with Myc-MIRO1<sup>Pex</sup>. For each cell analysed, 250 stacks of 9 planes were obtained over time, and peroxisomes were detected and tracked using an automated algorithm. E, Quantitative analysis of peroxisome number (first stack of each tracked cell). In all cases, expression of Myc-MIRO1<sup>Pex</sup> significantly increased peroxisome number: C109-741  $\pm$  53 vs 1040  $\pm$  101, dPEX5-304  $\pm$  27 vs 710  $\pm$  51 and dPEX14-268  $\pm$  18 vs 457  $\pm$  58. Values represent mean  $\pm$  SEM of 24 to 29 cells from 3 independent experiments (\*  $P < .05$ ; \*\*  $P < .01$ ; \*\*\*  $P < .001$ ; one-way ANOVA with post hoc Tukey test vs controls). F, Percentage of fast moving peroxisomes per cell in control and Myc-MIRO1<sup>Pex</sup> expressing fibroblasts. In all cases, peroxisome motility was significantly increased upon MIRO1 expression: C109-4.51  $\pm$  0.43 vs 11.05  $\pm$  1.32, dPEX5-1.61  $\pm$  0.20 vs 8.25  $\pm$  1.17, dPEX14-3.36  $\pm$  0.30 vs 8.30  $\pm$  1.59. Values represent mean  $\pm$  SEM of 14 to 26 cells in 3 independent experiments. Bars, 20  $\mu\text{m}$  (overview), 5  $\mu\text{m}$  (magnification)



**FIGURE 3** Expression of MIRO1 increases the length of peroxisome elongations in dPEX5 patient fibroblasts. A and B, dPEX5 patient fibroblasts were transfected with Myc-MIRO1<sup>Pex</sup>, fixed and stained against (A) Myc and PEX14. The majority of observed elongations in fixed cells show an evenly distributed Myc-MIRO1<sup>Pex</sup> signal (arrowheads), likely originating from a large peroxisome as shown by the strong PEX14 staining at one of the extremities (arrowheads). B, dPEX5 cells were fixed and stained against PEX14 and TUBULIN. Elongated peroxisomal structures were usually found overlaying microtubules (arrowheads). C–E, dPEX5 patient fibroblasts were transfected with EGFP-ACBD5<sup>TMD-T</sup> (peroxisomal membrane marker) and Myc-MIRO1<sup>Pex</sup>. C, Time lapse of peroxisome elongation forming and retracting in a dPEX5 cell expressing EGFP-ACBD5<sup>TMD-T</sup> and Myc-MIRO1<sup>Pex</sup>. D, Kymograph of peroxisome elongation observed in C. Bars, 20 seconds (vertical), 5 μm (horizontal). E, Quantitative analysis of peroxisome elongation length in dPEX5 and dPEX14 cells. Expression of Myc-MIRO1<sup>Pex</sup> significantly increased the length of peroxisome elongations in dPEX5 cells ( $1.62 \pm 0.08$  vs  $2.21 \pm 0.15$ ), but not in dPEX14 cells ( $1.44 \pm 0.07$  vs  $1.47 \pm 0.09$ ). Values represent mean  $\pm$  SEM from 22 to 29 cells, 3 independent experiments (\*\*\*)  $P < .001$ ; two-tailed unpaired t test vs controls). Bars, 20 μm (overview), 5 μm (magnification)

rate  $\beta$  causes almost all elongations to divide soon after formation, so that increased elongation growth rate and lipid flow can only result in proliferation (Figures 2D and 4B(b)). Conversely, in COS-7 cells, MIRO1 overexpression results in peroxisomes moving to the cell periphery (Figures 1 and 4B(a)). We model this as an increase in  $v$  with no corresponding increase in lipid flow (eg, due to reduced peroxisome-ER contact). Since lipid flow cannot keep up with the increased elongation speed, there is little impact on morphology or number, in agreement with our experimental observations.

The peroxisome phenotype in PEX5 deficient cells can be captured in the model by reducing both the division rate  $\beta$  and the elongation speed  $v$  (Figure 4A(e)), resulting in fewer and larger peroxisomes. This is in line with compromised peroxisome division and proliferation due to impaired peroxisomal lipid metabolism.<sup>51</sup> Modelling overexpression of MIRO1 in PEX5 deficient cells (by also increasing  $v$  and decreasing  $\gamma$ ) recapitulates the phenotype we found experimentally, where a substantial proportion of peroxisomes contain long elongations (Figure 4A(f),B(c)). Interestingly, this indicates that, despite a lack of peroxisomal metabolism, peroxisomal membranes retain their plasticity allowing lipid flow and membrane growth. Peroxisome proliferation in those cells is likely impaired due to reduced division rates (eg, due to altered peroxisomal membrane lipid composition). Whereas expression of MIRO1 cannot fully restore division, this can be achieved by PEX11 $\beta$ , a key factor in peroxisomal membrane remodelling and division<sup>1</sup> (Figure 5A). Expression of PEX11 $\beta$ -EGFP in PEX5 deficient cells promoted peroxisome elongation and subsequent division (Figure 5A) confirming earlier reports that PEX11 $\beta$ -induced peroxisome proliferation is independent of peroxisomal metabolism.<sup>45,54</sup> As PEX11 $\beta$  also activates the fission GTPase Drp1,<sup>15</sup> it likely increases the division rate  $\beta$  as well as the elongation speed  $v$  and lipid flow rate.

In mammalian cells, peroxisomes can elongate independently of microtubules, and peroxisome elongation is promoted by microtubule-depolymerizing drugs.<sup>9,49</sup> This suggests that PEX11 $\beta$  and motor forces (eg, mediated by MIRO1) can act independently to promote peroxisome proliferation, but may cooperate under physiological conditions. This assumption is supported by live-cell imaging of peroxisome dynamics in COS-7 cells expressing PEX11 $\beta$ -EGFP (Figure 5B,C).<sup>14</sup> Similar to PEX5 deficient cells, PEX11 $\beta$ -EGFP expression results in the formation of membrane protrusions emanating from globular peroxisomes. Occasionally, these peroxisomes show directed, long-range movements with the linear protrusion leading (Figure 5C 28-40 seconds; Video S10). These structures resemble the globular peroxisomes and protrusions induced by MIRO1 via microtubule-dependent motor forces. Globular peroxisomes can become more static, either by docking to microtubules and/or tethering to other organelles such as the ER (66.2%  $\pm$  2.6% of peroxisomes in COS-7 cells are associated with the ER<sup>46</sup>; Figure 5C 42-54 seconds; Video S10). However, in contrast to the more static globular peroxisomes, the membrane protrusions show a more random, tentacle-like movement, which does not seem to be directed by microtubules (Figure 5C 42-54 seconds; Video S10). This type of movement likely allows the peroxisomes to efficiently explore the environment and to engage with other organelles while being attached. Peroxisomes can then detach again and continue to move

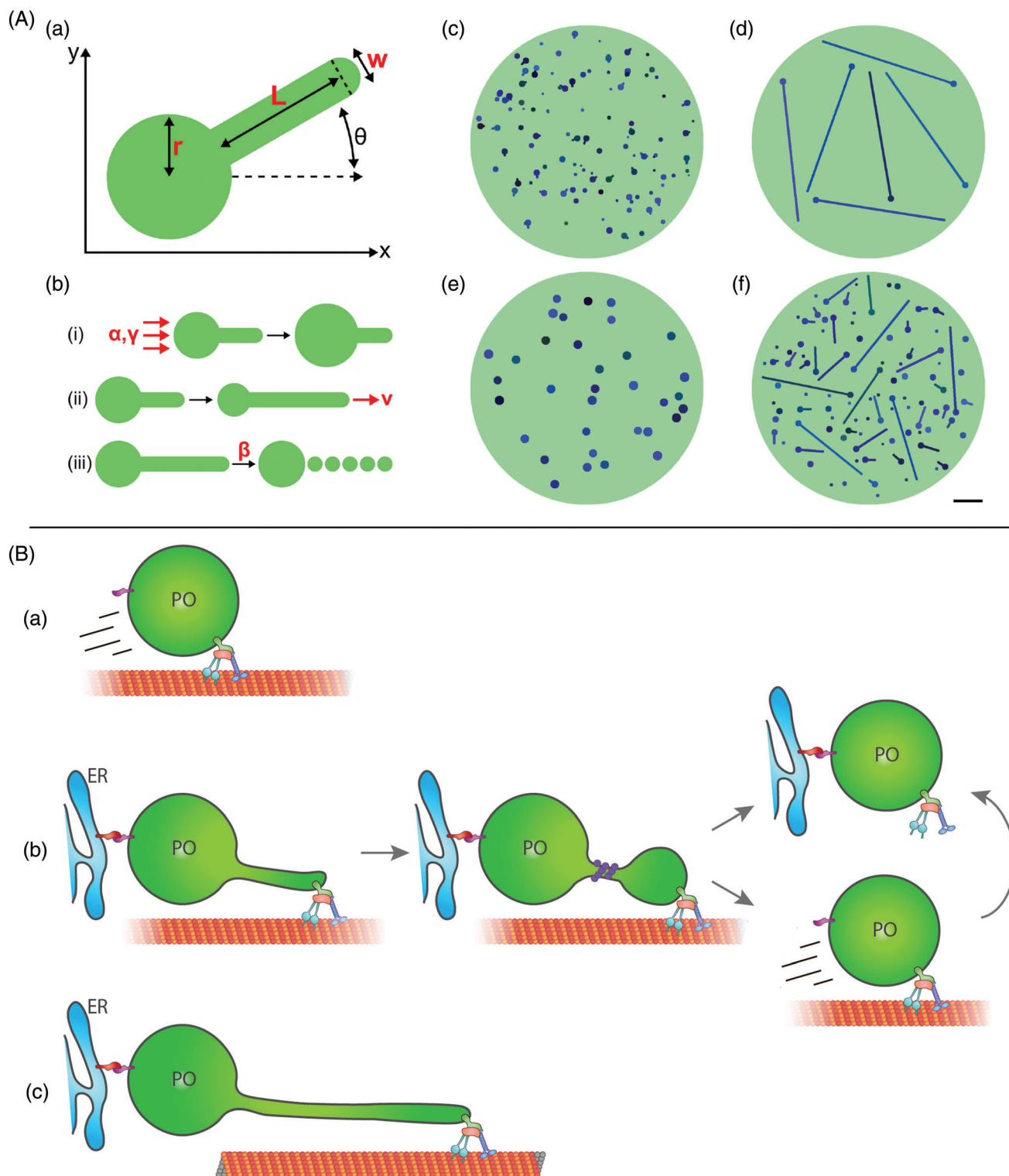
in a directed manner. Occasionally, membrane division is observed (Figure 5C 135-141 seconds; Video S10). These observations indicate that different, but cooperating mechanisms contribute to peroxisome dynamics and proliferation: PEX11 $\beta$  enables peroxisome membrane protrusion via its membrane deforming and scaffolding properties, and subsequently leads to division whereas MIRO1 on the other hand can elongate and divide peroxisomes by pulling forces via its interaction with microtubule-dependent motors. Both mechanisms can function independently, as peroxisomes can elongate and divide in the absence of microtubules, but adaptors such as MIRO1 and associated motors provide directionality to peroxisome membrane expansion and peroxisome movement.

### 3 | DISCUSSION

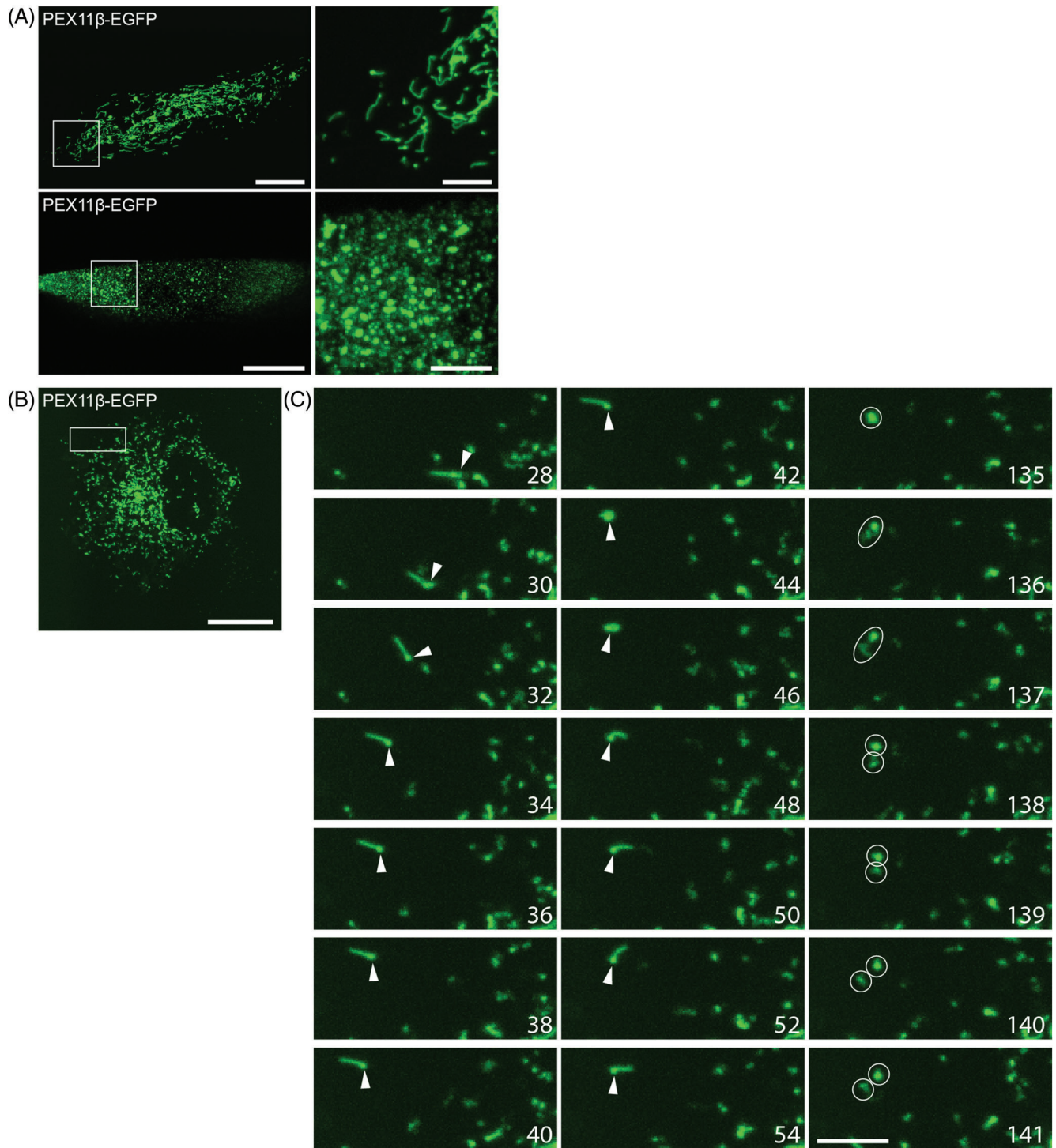
Our findings support a peroxisomal and mitochondrial localisation of MIRO1 and a role for MIRO1 in establishing peroxisome-motor protein associations in mammalian cells. As MIRO1 can alter peroxisome distribution and motility, it is likely one of the yet unidentified adaptors for microtubule-based peroxisome motility in mammalian cells. This assumption is further supported by recent findings showing that mitochondria and peroxisomes share many TA membrane proteins and their functions due to their close cooperation and co-evolution in mammalian cells.<sup>34</sup> During the submission of our work, Okumoto et al.<sup>55</sup> revealed that distinct MIRO1 splice variants show different targeting to mitochondria and peroxisomes in HEK cells, with MIRO1-variant 4 being more specific for peroxisomes. Peroxisomal MIRO1 also induced peroxisome accumulation and mediated long-range movement of peroxisomes along microtubules further supporting a role for MIRO1 in peroxisomal motility. In contrast to our findings, MIRO1-var1 localised primarily to mitochondria, which may be explained by the use of different cell lines or differences in expression levels of MIRO1.

We also show that peroxisome-targeted MIRO1 can be used as a tool to exert pulling forces at peroxisomes, and that MIRO1-mediated pulling forces have an impact on peroxisomal distribution, membrane dynamics and proliferation. These observations in combination with our mathematic model of peroxisome dynamics, shed light on the role of pulling forces in peroxisome formation by growth and division which have been controversial.<sup>9,17</sup> We show that MIRO1-mediated motor forces along microtubules can elongate and divide peroxisomes. As elongation and division can still occur in the absence of microtubules, we suggest that independent, but cooperative mechanisms exist, and that motor forces support membrane dynamics by providing directionality. This is now in agreement with observations in yeast, where actin-based, myosin-driven pulling forces cause peroxisome elongation and separation in dynamin mutants.<sup>56,57</sup> Our approaches also contribute to the understanding of the versatility of peroxisome morphology in mammalian cells. In our model, we develop basic principles for peroxisome dynamics which govern peroxisome morphology. This helps us to understand why peroxisomes in division-incompetent cells are highly elongated (due to continued lipid flow, eg, from the ER, in the absence of membrane fission), and





**FIGURE 4** A, Mathematical model of peroxisomal growth and division. (a) Each peroxisome is represented as a spherical body of radius  $r$  and a cylindrical elongation of length  $L$  and diameter  $w$ . (b) The 3 processes implemented in the model: (1) membrane lipid flow into the body with rate  $\alpha$  and lipid flow constant  $\gamma$ , (2) growth of the elongation at speed  $v$  and (3) division with rate per unit length  $\beta$ . (c) Snapshot from the model simulation of wild-type cells ( $\alpha = 75 \text{ nm}^2/\text{s}$ ,  $\beta = 2 \times 10^{-5}/\text{nm/s}$ ,  $v = 0.3 \text{ nm/s}$ ,  $\tau = 40 \text{ hours}$ ,  $\gamma = 2.4 \times 10^{-7}/\text{nm}^2$ ). (d) Snapshot from the simulation of dMff cells (with reduced division rate  $\beta = 5 \times 10^{-11}/\text{nm/s}$ ). (e) Snapshot from the simulation of dPex5 cells ( $\beta = 10^{-9}/\text{nm/s}$ ,  $v = 2 \times 10^{-4} \text{ nm/s}$ ). (f) Snapshot from overexpression of MIRO1 in dPex5 cells ( $\beta = 10^{-9}/\text{nm/s}$ ,  $v = 3 \text{ nm/s}$ ,  $\gamma = 1.2 \times 10^{-7}/\text{nm}^2$ ). Bar,  $1 \mu\text{m}$ . B, Schematic representation of the effects of MIRO1 on peroxisome dynamics and morphology. (a) Un-tethered peroxisomes move via the microtubule cytoskeleton in a MIRO1 dependent manner; (b) peroxisomes tethered to the ER are pulled by MIRO1-mediated motor forces and divide to form new peroxisomes; (c) defects in peroxisomal metabolism compromise MIRO1-mediated peroxisome division and proliferation resulting in elongated membrane protrusions



**FIGURE 5** PEX11 $\beta$  promotes peroxisome membrane elongation and division. (A) PEX5 deficient patient fibroblasts or (B-C) COS-7 cells were transfected with PEX11 $\beta$ -EGFP. A, PEX11 $\beta$ -EGFP induces peroxisome proliferation, leading to the formation of elongated peroxisomes (top), followed by their fission into numerous small peroxisomes (bottom). C, Time lapse of peroxisome elongation (left) and division (right). Note the directed, long-range movement of a peroxisome (arrow) with the linear protrusion leading (28-40 seconds). The same peroxisome becomes static, whereas the membrane protrusion exhibits a more random, tentacle-like movement (42-54 seconds) before it divides (135-141 seconds) (circles) (see also Video S10). For each cell analysed, 200 stacks of 9 planes were obtained over time. Time in seconds. Bars, 20  $\mu$ m (overview), 5  $\mu$ m (magnification)

why MIRO1-mediated pulling forces can proliferate peroxisomes in fibroblasts (due to peroxisome-ER tethers which prevent movement to the cell periphery). It also contributes to our understanding of peroxisome phenotypes in disease, eg, in PEX5 deficient cells from Zellweger patients. Here, metabolically compromised peroxisomes

retain their plasticity and can elongate via MIRO1-mediated pulling forces, but proliferation is reduced, likely due to altered membrane lipids.<sup>51</sup>

Despite their fundamental importance to cell physiology, the mechanisms that mediate and regulate peroxisomal membrane

dynamics and abundance in humans are poorly understood. Our study aids in understanding these mechanisms which is not only important for comprehending fundamental physiological processes but also for understanding pathogenic processes in disease aetiology.

## 4 | MATERIALS AND METHODS

### 4.1 | Plasmids and antibodies

For cloning of peroxisome-targeted MIRO1, the C-terminal TMD and tail of Myc-MIRO1 were exchanged by a PEX26/ALDP fragment previously shown to target proteins to the peroxisomal membrane.<sup>39</sup> See Table S1 for details of plasmids used in this study, Table S2 for plasmids generated in this study and Table S3 for details of primers used. All constructs produced were confirmed by sequencing (Eurofins Genomics). Details on all antibodies used in this study can be found in Table S4.

### 4.2 | Cell culture and transfection

COS-7 cells (American Type Culture Collection (Rockville, MD) [ATCC] CRL-1651), human control skin fibroblasts (C109), PEX5 and PEX14 deficient fibroblasts (provided by H. Waterham, AMC, University of Amsterdam, NL and M. Franssen, KU Leuven, BE) were cultured in DMEM, high glucose (4.5 g/L) supplemented with 10% FBS, 100 U/mL penicillin and 100 µg/mL streptomycin at 37°C with 5% CO<sub>2</sub> and 95% humidity. WT and MIRO1 KO mouse embryonic fibroblasts (MEF) (provided by J. Shaw, University of Utah, USA) were cultured in the same media and supplemented with β-mercaptoethanol at a final concentration of 50 µM. COS-7 cells were transfected using TurboFect (Thermo Fisher Scientific). To analyse the effects of microtubule depolymerisation, cells were treated 24 hours after transfection with 10 µM nocodazole (10 mM stock in dimethyl sulphoxide [DMSO]) and incubated for 1 or 4 hours before being fixed. Control cells were incubated with the same volume of DMSO as that used to dissolve nocodazole (maximum 0.1% vol/vol). Fibroblasts were transfected by microporation using the Neon Transfection System (Thermo Fisher Scientific) following the manufacturer's protocol. In short, cells (seeded 24 hours prior to transfection) were washed once with PBS and trypsinized using TrypLE Express. Trypsinized cells were resuspended in complete media without antibiotics and centrifuged for 3 minutes at 1000 rpm, and the pellet washed with PBS. The cells were once again centrifuged and carefully resuspended in 10 µL Buffer R. For each condition, 10<sup>5</sup> cells were mixed with the DNA construct (1–2 µg). Cells were microporated using a 10 µL Neon tip with the following settings: 1700 V, 20 ms, 1 pulse (human fibroblasts); 1350 V, 30 ms, 1 pulse (MEFs). Microporated cells were immediately seeded into plates with pre-warmed complete medium without antibiotics and incubated at 37°C with 5% CO<sub>2</sub> and 95% humidity. For live-cell imaging, cells were co-transfected with a fluorescent peroxisome marker (EGFP-SKL for COS-7 and EGFP-ACBD5<sup>TMD-T</sup> for fibroblasts) at a 1:2 ratio with Myc-MIRO1<sup>Pex</sup>

plasmids. As peroxisomal matrix import is defective in PEX5 and PEX14 patient fibroblasts, we used a fusion of EGFP and the TMD/tail region of ACBD5 (EGFP-ACBD5<sup>TMD-T</sup>) to label the peroxisomal membrane in control and patient cells.

### 4.3 | Immunofluorescence and microscopy

Cells were processed for immunofluorescence 24 or 48 hours after transfection. Cells grown on glass coverslips were fixed for 20 minutes with 4% paraformaldehyde (PFA) in PBS (pH 7.4), permeabilized with 0.2% Triton X-100 for 10 minutes and blocked with 1% BSA for 10 minutes. To visualise both peroxisomes and the microtubule network, cells were fixed for 10 minutes with 4% PFA followed by 5 minutes with ice-cold methanol. Blocked cells were sequentially incubated with primary and secondary antibodies for 1 hour in a humid chamber (Table S4). Coverslips were washed with ddH<sub>2</sub>O to remove PBS and mounted with Mowiol medium on glass slides. All immunofluorescence steps were performed at room temperature and cells were washed 3 times with PBS between each individual step. Cell imaging was performed using an Olympus IX81 microscope equipped with an UPlanSApo 100×/1.40 oil objective (Olympus Optical). Digital images were taken with a CoolSNAP HQ2 CCD camera and adjusted for contrast and brightness using the Olympus Soft Imaging Viewer software (Olympus Soft Imaging Solutions GmbH) and MetaMorph 7 (Molecular Devices). Confocal images were obtained using a Zeiss LSM 510 META inverted microscope equipped with a Plan Apochromat 63×/1.4 NA (oil/dic) objective (Carl Zeiss), using the Argon 488 nm and He 543 nm laser lines. Digital images were adjusted for contrast and brightness using the Zeiss LSM Image Browser software (Carl Zeiss MicroImaging GmbH). Live-cell imaging data was collected using an Olympus IX81 microscope equipped with a Yokogawa CSUX1 spinning disk head, CoolSNAP HQ2 CCD camera, 60×/1.35 oil objective. Digital images were taken and processed using VisiView software (Visitron Systems). For live-cell imaging, cells were plated in 3.5 cm diameter glass bottom dishes (Cellvis and MatTek). Prior to image acquisition, a controlled temperature chamber was set-up on the microscope stage at 37°C, as well as an objective warmer. During image acquisition, cells were kept at 37°C and in CO<sub>2</sub>-independent medium (HEPES buffered). For COS-7 cells, 500 stacks of 5 planes (0.5 µm thickness, 100 ms exposure) were taken in a continuous stream. For human fibroblasts, 250 stacks of 9 planes (0.5 µm thickness, 100 ms exposure) were taken in a continuous stream. All conditions and laser intensities were kept between experiments. For each condition analysed, a representative cell was selected and the acquired images were converted into a video at 10× the original speed.

### 4.4 | Peroxisome motility, number and length measurements

Peroxisomes were automatically detected and tracked using a customised in-house algorithm.<sup>41,46</sup> Briefly, each image was filtered using a scale-space Laplace of Gaussian filtering approach<sup>58,59</sup> over scales corresponding to the size range of peroxisomes. After filtering, a

threshold was determined using the median absolute deviation as a robust estimator of the background level,<sup>60</sup> and applied to the filter response to determine peroxisome positions. Once detected, peroxisomes were tracked using a global optimization subroutine (using a modified version of the Jonker-Volgenant algorithm).<sup>61</sup> Tracking results were manually verified for accuracy. For trajectory plots, 100 trajectories were retrieved for each condition by randomly selecting approximately 4 trajectories, of length at least 20 time-frames, from each data set. Next, the trajectories were re-centred such that each trajectory started at (0,0), and subsequently smoothed applying a simple moving-average algorithm using a Hann window. The first 20 time-frames for these trajectories were then plotted starting at a centre. For cumulative distribution function (CDF) plots, basic instantaneous trajectory speed profiles were estimated by calculating the distance moved between each time-point in the trajectory. These speeds were then pooled and converted into an ECDF. By pooling the speeds for all data sets for a given condition a single ECDF for each condition was generated. Trajectories for the tracked peroxisomes were analysed by splitting their instantaneous speeds into 2 groups, using a cut-off for linear motion speed of 0.24  $\mu\text{m/s}$ .<sup>42</sup> The relative populations of the 2 groups of peroxisome speeds were used as an indication of the amount of linear motion for each data set, and compared against all trajectories to obtain a percentage of microtubule-dependent motility per cell. The number of peroxisomes per cell was obtained from the motility analysis output, and determined by the detected peroxisome from the first frame of each analysed cell. Peroxisome protrusion lengths were obtained from live-cell imaging data and manually measured using MetaMorph 7. Each observed protrusion was measured at the longest point of extension. Kymographs were generated using ImageJ (developed at the National Institutes of Health).

#### 4.5 | Immunoprecipitation

For immunoprecipitation experiments Myc-MIRO1 WT and HA-PEX19 were expressed in COS-7 cells. After 48 hours cells were washed in PBS and incubated with 1 mM DSP followed by quenching with 100 mM Tris pH 7.4. After crosslinking cells were lysed in ice-cold lysis buffer (25 mM Tris-HCl pH 7.5, 150 mM NaCl, 0.5% Triton X-100, 1 mM phenylmethylsulfonyl fluoride (PMSF) and protease inhibitor cocktail). Undissolved material was pelleted by centrifugation at 15000g. The supernatant was mixed with Myc-antibody coupled agarose beads and incubated for 2 hours at 4°C. Beads were subsequently washed extensively with lysis buffer by quick centrifugations at 12000g and by incubating in a rotating shaker for 15 minutes at 4°C. Bound proteins were eluted with 50 mM NaOH and the eluted protein was denatured in Laemmli buffer for 10 minutes at 95°C. Immunoprecipitates and total lysates were analysed by Western immunoblotting.

#### 4.6 | Mathematical modelling

Each peroxisome was described by its body radius  $r$  and elongation length  $L$ . Simulations were started with 250 peroxisomes, each with a random initial radius and no elongation. After each time step ( $\Delta t = 1$

second), we implemented 3 processes. First, lipid flow from the ER into the body: the body surface area was increased by  $\alpha\Delta t$  with probability  $e^{-\gamma A}$ , where  $A$  is the total area of all peroxisomes. Second, if the body radius was above  $r_{\text{min}}$ , the elongation was increased by length  $v\Delta t$ , with the extra elongation area taken from the body. Third, when the elongation length was longer than  $L_{\text{min}}$ , peroxisomes underwent division with probability  $\beta L\Delta t$ . In addition, during each time step, each peroxisome had probability  $\Delta t/\tau$  of being removed by turnover. Simulations were carried out in C++ and MATLAB. See Supporting information for full details. The MATLAB code can be made available upon request.

#### 4.7 | Statistical analyses

For quantitative analysis of the effect of MIRO1 expression on peroxisome distribution, motility and number, at least 3 independent experiments were carried out. Statistical analyses were performed using Microsoft Excel and GraphPad Prism 5 software. Data are presented as means  $\pm$  SEM. Two-tailed unpaired t tests and one-way ANOVA with post hoc Tukey tests were used to determine statistical differences against control values. \*  $P < .05$ , \*\*  $P < .01$ , \*\*\*  $P < .001$ .

#### ACKNOWLEDGMENTS

We thank all colleagues who provided cell lines, plasmids and antibodies (see Tables S1-S4). This work was supported by Biotechnology and Biological Sciences Research Council (BB/K006231/1, BB/N01541X/1) and FCT (PTDC/BIA-BCM/118605/2010) to M.S.; D.M.R., M.S. and J.M. were supported by a Wellcome Trust Institutional Strategic Support Award (WT105618MA; WT097835MF) and D.M.R. by the Medical Research Council (MR/P022405/1). D.R. and A.G. were supported by personal fellowship grants from the Portuguese Foundation for Science and Technology (FCT) (SFRH/BPD/77619/2011; SFRH/BD/81223/2011) under the scope of "Programa Operacional Temático Factores de Competitividade" (COMPETE) of "Quadro Comunitário de Apoio III" and co-financed by Fundo Comunitário Europeu (FEDER). The authors declare no conflict of interest.

#### Author contributions

J.B.P., T.A.S., A.G. performed experiments and analysed data; M.S., I.G.C., J.M., J.L.C., D.M.R., D.R. conceived the project, performed experiments, analysed data; M.S., I.G.C., J.L.C., J.M. and D.M.R. wrote the manuscript; all authors contributed to methods.

#### ORCID

Inês G. Castro  <http://orcid.org/0000-0003-4669-985X>

Jeremy Metz  <http://orcid.org/0000-0002-8099-8776>

Joseph L. Costello  <http://orcid.org/0000-0002-2867-1864>

Josiah B. Passmore  <https://orcid.org/0000-0001-7791-3439>

Daniela Ribeiro  <http://orcid.org/0000-0003-3397-0460>

Michael Schrader  <http://orcid.org/0000-0003-2146-0535>

## REFERENCES

- Schrader M, Costello JL, Godinho LF, Azadi AS, Islinger M. Proliferation and fission of peroxisomes - an update. *Biochim Biophys Acta*. 2016;1863:971-983.
- Waterham HR, Ferdinandusse S, Wanders RJA. Human disorders of peroxisome metabolism and biogenesis. *Biochim Biophys Acta*. 2016;1863(5):922-933.
- Nordgren M, Fransen M. Peroxisomal metabolism and oxidative stress. *Biochimie*. 2014;98(1):56-62.
- Schrader M, Godinho LF, Costello JL, Islinger M. The different facets of organelle interplay—an overview of organelle interactions. *Front Cell Dev Biol*. 2015;3:56.
- Shai N, Schuldiner M, Zalckvar E. No peroxisome is an island - peroxisome contact sites. *Biochim Biophys Acta*. 2016;1863(5):1061-1069.
- Valm AM, Cohen S, Legant WR, et al. Applying systems-level spectral imaging and analysis to reveal the organelle interactome. *Nature*. 2017;546(7656):162-167.
- Fagarasanu A, Mast FD, Knobloch B, Rachubinski RA. Molecular mechanisms of organelle inheritance: lessons from peroxisomes in yeast. *Nat Rev Mol Cell Biol*. 2010;11(9):644-654.
- Sparkes I, Gao H. Plant peroxisome dynamics: movement, positioning and connections. *Molecular Machines Involved in Peroxisome Biogenesis and Maintenance*. Springer, Vienna; 2014:461-477.
- Schrader M, Burkhardt JK, Baumgart E, et al. Interaction of microtubules with peroxisomes. Tubular and spherical peroxisomes in HepG2 cells and their alterations induced by microtubule-active drugs. *Eur J Cell Biol*. 1996;69:24-35.
- Schrader M, King SJ, Stroh TA, Schroer TA. Real time imaging reveals a peroxisomal reticulum in living cells. *J Cell Sci*. 2000;113:3663-3671.
- Wiemer EAC, Wenzel T, Deerinck TJ, Ellisman MH, Subramani S. Visualization of the peroxisomal compartment in living mammalian cells: dynamic behavior and association with microtubules. *J Cell Biol*. 1997;136(1):71-80.
- Rapp S, Saffrich R, Anton M, et al. Microtubule-based peroxisome movement. *J Cell Sci*. 1996;109:837-849.
- Schrader M, Reuber BE, Morrell JC, et al. Expression of PEX11 $\beta$  mediates peroxisome proliferation in the absence of extracellular stimuli. *J Biol Chem*. 1998;273(45):29607-29614.
- Delille HK, Agricola B, Guimaraes SC, et al. Pex11 $\beta$ -mediated growth and division of mammalian peroxisomes follows a maturation pathway. *J Cell Sci*. 2010;123(Pt 16):2750-2762.
- Williams C, Opalinski L, Landgraf C, et al. The membrane remodeling protein Pex11p activates the GTPase Dnm1p during peroxisomal fission. *Proc Natl Acad Sci U S A*. 2015;112(20):6377-6382.
- Asare A, Levorso J, Fuchs E. Coupling organelle inheritance with mitosis to balance growth and differentiation. *Science*. 2017;355(6324):eaah4701. <https://doi.org/10.1126/science.aah4701>.
- Schrader M, Fahimi HD. Growth and division of peroxisomes. *Int Rev Cytol*. 2006;255(6):237-290.
- Chang J, Mast FD, Fagarasanu A, et al. Pex3 peroxisome biogenesis proteins function in peroxisome inheritance as class V myosin receptors. *J Cell Biol*. 2009;187(2):233-246.
- Otzen M, Rucktäschel R, Thoms S, et al. Pex19p contributes to peroxisome inheritance in the association of peroxisomes to Myo2p. *Traffic*. 2012;13(7):947-959.
- Dietrich D, Seiler F, Essmann F, Dodt G. Identification of the kinesin KifC3 as a new player for positioning of peroxisomes and other organelles in mammalian cells. *Biochim Biophys Acta*. 2013;1833(12):3013-3024.
- Fransson A, Ruusala A, Aspenström P. Atypical Rho GTPases have roles in mitochondrial homeostasis and apoptosis. *J Biol Chem*. 2003;278(8):6495-6502.
- MacAskill AF, Rinholm JE, Twelvetrees AE, et al. Miro1 is a calcium sensor for glutamate receptor-dependent localization of mitochondria at synapses. *Neuron*. 2009;61(4):541-555.
- Saotome M, Safiulina D, Szabadkai G, et al. Bidirectional Ca<sup>2+</sup>-dependent control of mitochondrial dynamics by the Miro GTPase. *Proc Natl Acad Sci U S A*. 2008;105(52):20728-20733.
- van Spronsen M, Mikhaylova M, Lipka J, et al. TRAK/Milton Motor-adaptor proteins steer mitochondrial trafficking to axons and dendrites. *Neuron*. 2013;77(3):485-502.
- Wang X, Schwarz TL. The mechanism of Ca<sup>2+</sup>-dependent regulation of kinesin-mediated mitochondrial motility. *Cell*. 2009;136(1):163-174.
- Devine MJ, Birsa N, Kittler JT. Miro sculpts mitochondrial dynamics in neuronal health and disease. *Neurobiol Dis*. 2016;90:27-34.
- Yamaoka S, Hara-Nishimura I. The mitochondrial Ras-related GTPase Miro: views from inside and outside the metazoan kingdom. *Front Plant Sci*. 2014;5:350.
- Klosowiak JL, Focia PJ, Chakravarthy S, Landahl EC, Freymann DM, Rice SE. Structural coupling of the EF hand and C-terminal GTPase domains in the mitochondrial protein Miro. *EMBO Rep*. 2013;14(11):968-974.
- Schuler M-H, Lewandowska A, Caprio GD, et al. Miro1-mediated mitochondrial positioning shapes intracellular energy gradients required for cell migration. *Mol Biol Cell*. 2017;28(16):2159-2169.
- Koch A, Yoon Y, Bonekamp NA, Mcniven MA, Schrader M. A role for Fis1 in both mitochondrial and peroxisomal fission in mammalian cells. *Mol Biol Cell*. 2005;16:5077-5086.
- Delille HK, Schrader M. Targeting of hFis1 to peroxisomes is mediated by Pex19p. *J Biol Chem*. 2008;283(45):31107-31115.
- Gandre-Babbe S, van der Bliek AM. The novel tail-anchored membrane protein Mff controls mitochondrial and peroxisomal fission in mammalian cells. *Mol Biol Cell*. 2008;19:2402-2412.
- Huber N, Guimaraes SC, Schrader M, Suter U, Niemann A. Charcot-Marie-Tooth disease-associated mutants of GDAP1 dissociate its roles in peroxisomal and mitochondrial fission. *EMBO Rep*. 2013;14(6):545-552.
- Costello JL, Castro IG, Camoes F, et al. Predicting the targeting of tail-anchored proteins to subcellular compartments in mammalian cells. *J Cell Sci*. 2017;130:1675-1687.
- Wiese S, Gronemeyer T, Ofman R, et al. Proteomics characterization of mouse kidney peroxisomes by tandem mass spectrometry and protein correlation profiling. *Mol Cell Proteomics*. 2007;6(12):2045-2057.
- Jadot M, Boonen M, Thirion J, et al. Accounting for protein subcellular localization: a compartmental map of the rat liver proteome. *Mol Cell Proteomics*. 2017;16(2):194-212.
- Huttlin EL, Ting L, Bruckner RJ, et al. The BioPlex network: a systematic exploration of the human interactome. *Cell*. 2015;162(2):425-440.
- Fransson A, Ruusala A, Aspenström P. The atypical Rho GTPases Miro-1 and Miro-2 have essential roles in mitochondrial trafficking. *Biochem Biophys Res Commun*. 2006;344(2):500-510.
- Halbach A, Landgraf C, Lorenzen S, et al. Targeting of the tail-anchored peroxisomal membrane proteins PEX26 and PEX15 occurs through C-terminal PEX19-binding sites. *J Cell Sci*. 2006;119(Pt 12):2508-2517.
- Lin C, Schuster M, Guimaraes SC, et al. Active diffusion and microtubule-based transport oppose myosin forces to position organelles in cells. *Nat Commun*. 2016;7:11814.
- Metz J, Castro IG, Schrader M. Peroxisome motility measurement and quantification assay. *Bio Protoc*. 2017;7(17).
- Bonekamp NA, Sampaio P, de Abreu FV, Lüers GH, Schrader M. Transient complex interactions of mammalian peroxisomes without exchange of matrix or membrane marker proteins. *Traffic*. 2012;13(7):960-978.
- Nguyen TT, Oh SS, Weaver D, et al. Loss of Miro1-directed mitochondrial movement results in a novel murine model for neuron disease. *Proc Natl Acad Sci*. 2014;111(35):E3631-E3640.
- Guimaraes SC, Schuster M, Bielska E, et al. Peroxisomes, lipid droplets, and endoplasmic reticulum "hitchhike" on motile early endosomes. *J Cell Biol*. 2015;211(5):945-954.
- Nguyen T, Bjorkman J, Paton BC, Crane DI. Failure of microtubule-mediated peroxisome division and trafficking in disorders with reduced peroxisome abundance. *J Cell Sci*. 2006;119(Pt 4):636-645.
- Costello JL, Castro IG, Hacker C, et al. ACBD5 and VAPB mediate membrane associations between peroxisomes and the ER. *J Cell Biol*. 2017;216(2):331-342.

47. Bharti P, Schliebs W, Schievelbusch T, et al. PEX14 is required for microtubule-based peroxisome motility in human cells. *J Cell Sci.* 2011;124(Pt 10):1759-1768.
48. Mathur J, Mammone A, Barton KA. Organelle extensions in plant cells. *J Integr Plant Biol.* 2012;54(11):851-867.
49. Passmore JB, Pinho S, Gomez-Lazaro M, Schrader M. The respiratory chain inhibitor rotenone affects peroxisomal dynamics via its microtubule-destabilising activity. *Histochem Cell Biol.* 2017;148(3):331-341.
50. Santos MJ, Imanaka T, Peroxisomal Integral LPB. Membrane proteins in control and Zellweger fibroblasts. *J Biol Chem.* 1988;263(21):10502-10509.
51. Itoyama A, Honsho M, Abe Y, Moser A, Yoshida Y, Fujiki Y. Docosa-hexaenoic acid mediates peroxisomal elongation, a prerequisite for peroxisome division. *J Cell Sci.* 2012;125(Pt 3):589-602.
52. Koch J, Feichtinger RG, Freisinger P, et al. Disturbed mitochondrial and peroxisomal dynamics due to loss of MFF causes Leigh-like encephalopathy, optic atrophy and peripheral neuropathy. *J Med Genet.* 2016;53(4):270-278.
53. Shamseldin HE, Alshammari M, Al-Sheddi T, et al. Genomic analysis of mitochondrial diseases in a consanguineous population reveals novel candidate disease genes. *J Med Genet.* 2012;49(4):234-241.
54. Li X, Gould SJ. PEX11 promotes peroxisome division independently of peroxisome metabolism. *J Cell Biol.* 2002;156(4):643-651.
55. Okumoto K, Ono T, Toyama R, Shimomura A, Nagata A, Fujiki Y. New splicing variants of mitochondrial Rho GTPase-1 (Miro1) transport peroxisomes. *J Cell Biol.* 2017;jcb.201708122.
56. Hoepfner D, van den Berg M, Philippsen P, Tabak HF, Hettema EH. A role for Vps1p, actin, and the Myo2p motor in peroxisome abundance and inheritance in *Saccharomyces cerevisiae*. *J Cell Biol.* 2001;155(6):979-990.
57. Nagotu S, Saraya R, Otzen M, Veenhuis M, van der Klei IJ. Peroxisome proliferation in *Hansenula polymorpha* requires Dnm1p which mediates fission but not de novo formation. *Biochim Biophys Acta.* 2008;1783(5):760-769.
58. Lindeberg T. Feature detection with automatic scale selection. *Int J Comput Vis.* 1998;30(2):79-116.
59. Lindeberg T. *Scale-Space Theory in Computer Vision*. Vol 256. Springer Science & Business Media, Dordrecht; 1994.
60. Murtagh F, Starck J-L. Image processing through multiscale analysis and measurement noise modeling. *Stat Comput.* 2000;10(2):95-103.
61. Jonker R, Volgenant A. A shortest augmenting path algorithm for dense and sparse linear assignment problems. *Comput Secur.* 1987;38(4):325-340.

## SUPPORTING INFORMATION

Additional Supporting Information may be found online in the supporting information tab for this article.

**How to cite this article:** Castro I, Richards DM, Metz J, et al. A role for Mitochondrial Rho GTPase 1 (MIRO1) in motility and membrane dynamics of peroxisomes. *Traffic.* 2018;19:229-242. <https://doi.org/10.1111/tra.12549>